

# Triggered star formation in Bright Rimmed Clouds: The Eagle Nebula revisited

J.Miao<sup>1\*</sup>, Glenn J.White<sup>1</sup>, R.Nelson<sup>2</sup>, M.Thompson<sup>3</sup>, L.Morgan<sup>1</sup>

<sup>1</sup>*Centre for Astrophysics & Planetary Science, School of Physical Science, University of Kent, Canterbury, Kent CT2 7NR, UK*

<sup>2</sup>*School of Mathematical Sciences, Queen Mary, University of London, Mile End Road, London E1 4NS, UK*

<sup>3</sup>*School of Physics Astronomy & Maths, University of Hertfordshire, College Lane, Hatfield, AL10 9AB, UK*

Received date / Accepted date

## ABSTRACT

A three dimensional Smoothed Particle Hydrodynamical (SPH) model has been extended to study the radiative driven implosion effect of massive stars on the dynamical evolutions of surrounding molecular clouds. The new elements in the upgraded code are the inclusion of Lyman continuum in the incident radiation flux and the treatment of hydrogen ionisation process; introducing ionisation heating & recombination cooling effects; and adding a proper description of the magnetic and turbulent pressures to the internal pressure of the molecular cloud. This extended code provides a realistic model to trace not only the dynamical evolution of a molecular cloud, but also can be used to model the kinematics of the ionisation & shock fronts and the photo-evaporating gas surrounding the molecular cloud, which the previous code is unable to deal with.

The application of this newly developed model to the structure of the middle Eagle Nebula finger suggests that the shock induced by the ionising radiation at the front side of the head precedes an ionisation front moving towards the center of the core, and that the core at the fingertip is at transition stage evolving toward a state of induced star formation. The dynamical evolution of the velocity field of the simulated cloud structure is discussed to illustrate the role of the self-gravity and the different cloud morphologies which appear at different stages in the evolutionary process of the cloud. The motion of the ionisation front and the evaporating gas are also investigated. The modelled gas evaporation rate is consistent with that of current other models and the density, temperature and chemical profiles are agreement with the observed values.

The relative lifetimes of different simulated cloud morphologies suggests a possible answer to the question of why more bright-rimmed clouds are observed to possess a flat-core than an elongated-core morphology.

**Key words:** star: formation – ISM: evolution – ISM: HII regions – ISM: kinematics and dynamics – radiative transfer.

## 1 INTRODUCTION

The Eagle Nebula (M16) presents an excellent laboratory in which to study the influence on star formation due to the presence of nearby massive stars, which can lead to radiative implosion of surrounding molecular cores and the initiation of secondary star formation (Bertoldi 1989; Lefloch & Lazareff 1994). The intriguing structures in the heads of the Elephant Trunks in the Eagle Nebula have inspired many studies. A comprehensive survey conducted by Hester et al. (1996) using the HST Wide Field and Planetary Camera (WFPC2) resolved a number of Evaporating Gaseous Globules (EGGs) at the tip of finger-like features protruding from columns of cold gas and dust of the Eagle Nebula (Hester et al. 1996).

More investigations on the physical characteristics and the future evolution of the head structures have also been carried out since then (White et al. 1999; Williams et al. 2001; Fukuda et al. 2002; Sugitani et al. 2002; Thompson et al. 2002; Urquhart et al. 2003).

In one of our early papers (White et al. 1999), we reported molecular line, millimetre/submillimetre continuum, and mid-IR observations of this region. The steady state of the head structure of the middle finger of the Eagle Nebula was estimated using a SPH model which included a simple treatment of an isotropic FUV radiation field ( $6.5 < h\nu < 13.6$  eV). The comparison of the estimated steady state of the head structure of the middle finger with the observed data suggested that the FUV ionisation induced shock might have not passed the core at the middle fingertip, so that the head structure of the fingertip could not be taken as the remains of radiatively driven implosion. The observations revealed that the core

\* E-mail: j.miao@kent.ac.uk

structure shows the characteristics similar to those expected in the earliest stages of protostellar formation, therefore it was suspected that the head structure of the middle finger in the Eagle Nebula might evolve from a large and dense structure which existed prior to the expansion of the HII region.

Recently there have been other observations that have supported the idea of triggered protostellar formation at the tip of the middle finger, following the interaction of the natal molecular cloud with the ionising radiation from the nearby OB stars (Fukuda et al. 2002; Mcgaughrean & Andersen 2002; Sugitani et al. 2002; Thompson et al. 2002). The question is whether or not UV radiation from the nearby massive stars could trigger the collapse of the head structures in Eagle Nebula and lead to the next generation of star formation. The challenge is to develop theoretical models that provide a reliable description of the dynamical evolution of these clumpy structures and which can trace back the history of the clumps, accommodate the current observations, and predict the future evolution of these fingertip structures.

A precise description of the genesis and the future evolution of the head structures such as those of the Eagle Nebula fingers requires a more rigorous dynamical modelling which should include Lyman continuum in the external radiation field, since hydrogen ionisation ought to play a dominant role in the dynamical evolution of the molecular cloud structures like those in Eagle Nebula.

A substantial amount of theoretical work has already been carried out to investigate the evolution of dense, gaseous clumps which are in the vicinity of massive OB stars. These include the Radiatively Driven Implosion (RDI) mechanism (Bertoldi 1989) which was developed using an approximate analytical solution for the evolution of a spherical symmetric neutral cloud subject to the radiation of a newly formed nearby star; and the cometary globule model (Lefloch & Lazareff 1994, 1995), which describes the dynamical evolution of a neutral globule illuminated by the ionising radiation of OB stars based on 2-D hydrodynamical simulations. Although these 2-D models successfully reproduced some of the observed characteristics of objects influenced by nearby massive stars, they did not adequately include self-gravity (Bertoldi 1989), nor self-consistently treat the chemistry and thermal evolution (Lefloch & Lazareff 1994, 1995). Consequently they are unable to deal with the details of triggered star formation by UV radiation.

Williams et al. (2001) presented a 2-D (i.e., cylindrical symmetry of the cloud structure is used) hydrodynamical simulation of the evolution of photoionised clumps with similar characteristics to those found in the Eagle Nebula. The simulated results over a variety of initial conditions proposed a different evolutionary scenario from that of White et al. (1999) for the head structures, suggesting that the head structures at the tips of the Eagle Nebula trunks may have already survived the propagating shock induced by the external UV radiation field and are in a near-equilibrium state about  $10^5$  years later. In this modelling, self-gravity of the molecular gas was also not included.

The existing discrepancy in the descriptions of the structure of the heads at the finger tips and the recently reported new observations on the finger tips' structure suggests the necessity of revisiting the issue of UV radiation triggered star formation at these fingertips. In order to do this, a self-consistent and comprehensive 3-D BRCs' model is required which could be used to study the UV radiation triggered star formation in BRCs and which more generally can be used to describe observations in all of BRCs, proplyds and HII regions, to meet with the ever-increasing interest in the investigation of the nature of BRCs and proplyds in HII regions. It

is obviously seen from the above that this fully 3-D BRCs model should be able to self-consistently and simultaneously treat the self-gravity, thermal evolution, radiative transfer and chemistry. Therefore it is our intent to develop the first self-consistent and comprehensive 3-D BRCs's model based on a previous 3-D SPH code, which was originally developed to investigate the evolution of isolated molecular clouds under the effect of the interstellar medium radiation (Nelson & Langer 1997).

In the following sections in the present paper we will firstly present an outline for the previous 3-D SPH model and then introduce new elements necessary for simulating the evolution of BRCs. The simulation results will be discussed and compared with observations, and the evolutionary of the simulated cloud structure will be investigated. A comparison of the results with those based on the previous code is made and then we infer the future evolution of the Eagle Nebula finger from its current state. Based on the good agreement between simulations and observations, a reasonable explanation for the observed unbalanced numbers between the flat-core and elongated-core BRCs is proposed.

## 2 THE THREE DIMENSIONAL SPH MODELLING

The physical properties of the head structure of the Eagle Nebula presented in our previous paper (White et al. 1999) was based on the Smoothed Particle Hydrodynamics (SPH) code developed by Nelson & Langer (1997), which self-consistently treats the self-gravitation, chemical and thermal evolution in the molecular cloud. Starting with a cylindrical finger of radius 0.1 pc with a spherical molecular cloud of  $31 M_{\odot}$  at its head, which is under the effect of a FUV radiation field (with photon energy lower than 13.6 eV and enhanced from the +z-direction). Based on an assumed static density distribution (i.e., under equilibrium assumption), the temperature and chemical distributions, after the FUV radiation is switched on for  $10^5$  years, showed similar characteristics to observations of the middle finger. However the detailed and accurate description on the whole dynamical evolution, especially on the genesis and future evolution of the observed structures was not discussed at that time, since the original SPH code did not include the hydrogen ionising influence of the Lyman continuum radiation ( $h\nu \geq 13.6$  eV), the ionisation heating, recombination cooling or the relevant radiative transfer process. These are clearly important since the effect of the UV radiation of nearby massive stars on their surrounding molecular clouds tells us that hydrogen ionisation is one of the most important physical processes in radiation driven implosion models (Bertoldi 1989; Lefloch & Lazareff 1994; Williams et al. 2001).

Recently, (Kessel-Deynet & Burkert 2000, 2003) have developed a three-dimensional SPH model of the radiation-driven implosion of molecular cloud which includes both self-gravitation and hydrogen ionisation from nearby stars. Their model provided the first 3D SPH code to treat ionising radiation in turbulent astrophysical fluid flows, opening a wide field of applications involving feedback processes of young massive stars on their parental clouds. However a self-consistent treatment for the thermal evolution was not included in this model and the energy evolution was approximated by a simple linear function of the ionisation ratio  $x$ , i.e.,  $E = xE_{10000} + (1 - x)E_{cloud}$ , where  $E$  is the internal energy of a representative particle with ionisation ratio  $x$  ( $E_{10000}$  being the internal energy of a fully ionised particle at a temperature of 10000 K and  $E_{cloud}$  being the internal energy of a neutral particle at a temperature of 10 K). The absence of a self-consistent treatment of the ionisation heating and recombination cooling processes in

their model prevents a rigorous calculation of the physical properties of the cloud, such as gas temperature, density, sound velocity and pressure (Kessel-Deynet & Burkert 2000, 2003), which in fact can adequately be validated through observational data.

We therefore extend our previous code to include a wider range of UV radiation energy distributions, hydrogen ionisation, radiative transfer, ionisation heating and recombination cooling, to provide a more comprehensive and self-consistent investigation on the effect of radiation of massive stars on their parental molecular clouds.

## 2.1 The main components in the previous SPH code

A detailed description of the previous SPH code can be found in Nelson & Langer (1997) and White et al. (1999). Here we present a brief introduction of its main features for completeness. In the previous version of the code, the SPH numerical technique was employed to solve the following continuity, momentum and energy equations for a compressible fluid

$$\frac{d\rho}{dt} + \rho \nabla \cdot \mathbf{v} = 0 \quad (1)$$

$$\frac{d\mathbf{v}}{dt} = -\frac{1}{\rho} \nabla P - \nabla \Phi + \mathbf{S}_{\text{visc}} \quad (2)$$

$$\frac{d\mathcal{U}}{dt} + \frac{P}{\rho} \nabla \cdot \mathbf{v} = \frac{\Gamma - \Lambda}{\rho} \quad (3)$$

and the chemical rate equations take the general form:

$$\frac{dX_i}{dt} = nK_i \quad (4)$$

where  $\frac{d}{dt} = \frac{\partial}{\partial t} + \mathbf{v} \cdot \nabla$  denotes the convective derivative,  $\rho$  is the density,  $\mathbf{v}$  is the velocity,  $P$  is the pressure,  $\mathbf{S}_{\text{visc}}$  represents the viscous forces,  $\mathcal{U}$  is the internal energy per unit mass, and  $\Phi$  is the gravitational potential.  $\Gamma$  and  $\Lambda$  represent nonadiabatic heating and cooling functions respectively.

The heating function  $\Gamma$  in thermal modelling is mainly provided by the photoelectric emission of electrons from grains illuminated by the incident FUV ( $6.5 < h\nu < 13.6$  eV) component at the surface of the cloud. This is stronger on the surface facing toward the source star, and weaker on the shielded cloud surface since the latter is mainly from backscattered light by the surrounding interstellar medium and is 0.1–0.2 times that on the directly illuminated surface (Désert et al. 1990; Hurwitz et al. 1991), i.e., the FUV radiation flux incident the boundary of the cloud can be written as

$$J_{\text{FUV}}(r = R, \theta) = \begin{cases} 2000G_0 & 0^\circ \leq \theta \leq 90^\circ \\ 0.2 * 2000G_0 & 90^\circ \leq \theta \leq 180^\circ \end{cases}$$

where  $G_0$  is the standard interstellar UV field (Habing 1968) and  $\theta$  is the azimuthal angle in spherical coordinate. Heating of the gas is also affected by cosmic ray heating,  $\text{H}_2$  formation heating and gas-dust thermal exchange.

The cooling function  $\Lambda$  is affected by CO, CI, CII and OI line emission. The fractional abundance of main chemical species  $X_i$  in Equation (4) are for CO, CI, CII,  $\text{HCO}^+$ , OI,  $\text{H}_e^+$ ,  $\text{H}_3^+$ ,  $\text{OH}_x$ ,  $\text{CH}_x$ ,  $\text{M}^+$  and electrons;  $K_i$  is the associated chemical reaction rate and  $n$  is the total number density. Detailed formula for these physical and chemical processes can be found in papers of Nelson & Langer (1997) and White et al. (1999).

The dominant heating process included in the above is the photoelectric emission of electrons from dust grains by the incident FUV (1–13.6 eV), as the code was originally developed to

observe the influence of the interstellar radiation on the chemical and thermal evolution of an isolated molecular clouds, such as Bok globules. For the investigation of the influence of more intensive UV radiation from massive stars on the evolution of its surrounding objects, hydrogen ionisation heating will play a dominant role since the intensive Lyman continuum photons available in the radiative flux, and the much higher abundance of hydrogen atoms than that of grain particles. Therefore it is necessary to include the hydrogen ionisation process and the relevant heating and cooling process in order to fulfill our goal.

## 2.2 New elements

The new elements added into the above original code are solving for the ionising radiation transfer equation, hydrogen ionisation heating and electron recombination cooling. We also introduce a realistic description of the pressure of the molecular cloud by including the turbulent and magnetic pressures. More detailed descriptions are contained in the following sub-sections.

### 2.2.1 Ionising radiation transfer

Although Helium ionisation was included in the above chemical network, we could safely neglect it when dealing with the ionisation radiation transfer, ionisation heating and cooling for simplicity, because of the much lower abundance of the Helium compared to hydrogen atoms (Dyson & Williams 1997). The treatment of ionising radiation from nearby stars into the above SPH code is based on solving the following ionisation rate and radiative transfer equations,

$$\frac{dn_e}{dt} = I - \mathcal{R} \quad (5)$$

$$\frac{dJ}{dz} = -\sigma n(1-x)J \quad (6)$$

where  $n_e = xn$  is the electron density by ionising hydrogen atoms, and  $x$  is the ionisation fraction;  $I = \sigma n(1-x)J$  is the ionisation rate,  $J$  is the flux of Lyman continuum photons at the site and  $\sigma$  is the ionisation cross-section of hydrogen in the ground state.  $\mathcal{R} = n_e^2 \alpha_B = x^2 n^2 \alpha_B$  is the recombination rate, where  $\alpha_B$  is the effective recombination coefficient under the assumption of the 'on the spot' approximation (Dyson & Williams 1997). In its original definition, the recombination coefficient

$$\alpha = \sum_i \alpha_i$$

includes all of the individual recombination coefficients  $\alpha_i$  to the hydrogen atomic energy level  $i$ . In the 'on the spot' assumption, recombinations into the ground level ( $i = 1$ ) do not lead to any net effect on the change in ionisation rate, since the photons released from this recombination process are able to re-ionise other hydrogen atoms on the spot. Therefore  $\alpha_1$  can be neglected and the resulting net recombination coefficient can be written as

$$\alpha_B = \sum_{i=2}^{\infty} \alpha_i$$

The dependence of the recombination coefficient  $\alpha_B$  on the temperature can be expressed by Hummer & Seaton (1963),

$$\alpha_B = 1.627 \times 10^{-13} t_e^{-1/2} (1 - 1.657 \log_{10} t_e + 0.584 t_e^{1/3}) \quad (7)$$

where  $t_e = 10^{-4} T$  (T in K).

The equations 6 is numerically integrated at each time step and with the density distribution  $n_H(x, y, z)$  which resulted from the dynamical evolutions. where  $J_0$  is the flux of Lyman continuum photons at the surface the molecular cloud and we take the value  $J_0 = 1.5 \times 10^{11} \text{ cm}^{-2} \text{ s}^{-1}$ , which is the same as that used by Williams et al. (2001).

### 2.2.2 Ionisation heating and recombination cooling

The implementation of the thermal model for the ionisation process includes the energy input by photoionisation and energy loss by recombination. When an atom with ionisation energy  $E_1$  is ionised following the absorption of one photon of frequency  $\nu$  and energy  $E = h\nu$ , it releases one electron which carries the excess kinetic energy  $E_\nu - E_1$  which will be transferred to the gas through collisions with other gas particles. The resulting heating rate is described by the following equation

$$\Gamma_{\text{ionising}} = n(1-x)\sigma J k T_* \quad (8)$$

where  $k$  is the Boltzmann constant and  $T_*$  is expressed as (Cantó et al 1998)

$$T_* = T_{\text{eff}} \frac{x_0^2 + 4x_0 + 6}{x_0^2 + 2x_0 + 2} \quad (9)$$

where  $T_{\text{eff}}$  is the stellar temperature, and  $x_0 = (h\nu_0)/(kT_{\text{eff}})$  with  $\nu_0$  being the frequency of the Lyman limit.

When a free electron in the plasma is captured by a proton, a photon is emitted and an amount of energy  $E_1 + m_e v_e^2/2$  is removed from the internal energy of the gas. The cooling rate due to this process is (Hummer & Seaton 1963)

$$\Lambda_{\text{rec}} = \beta_B n^2 x^2 k T \quad (10)$$

where  $\beta_B = \alpha_B \times (1 + 0.158 t_e)$ .

### 2.2.3 Cooling by collisionally excited line radiation

Accompanying with the ionisation of hydrogen atoms, oxygen is ionised to  $\text{O}^+$  (OII) as well. Consequently, the collisional excitation of low-lying energy levels of OII makes a significant cooling effect in spite of OII's low abundance, since OII has energy levels with excitation potentials of the order of  $kT$ . We use the following simplified formula derived by Raga et al (2002) to calculate the cooling rate due to the collisional excitation of OII,

$$\Lambda_{\text{colli}} = \Lambda_{\text{colli}(1)} + \Lambda_{\text{colli}(2)} \quad (11)$$

with

$$\log_{10} \left[ \frac{\Lambda_{\text{colli}(1)}}{n_e n_{\text{OII}}} \right] = 7.9 t_1 - 26.8 \quad (12)$$

$$\log_{10} \left[ \frac{\Lambda_{\text{colli}(2)}}{n_e n_{\text{OII}}} \right] = 1.9 \frac{t_2}{|t_2|^{0.5}} - 20.5 \quad (13)$$

with  $t_1 = 1 - 2000 \text{ K}/T$  and  $t_2 = 1 - 5 \times 10^4 \text{ K}/T$  and  $n_{\text{OII}} = x n_{\text{O}}$ . The above formula is valid under the limit of low electron density  $n_e < 10^4 \text{ cm}^{-3}$ , which is true for the BRCs systems.

### 2.2.4 The pressure of the cloud and the boundary conditions

At the start of a simulation, the molecular cloud is assumed to have a spherical symmetry which is the general assumption adopted by most existing theoretical models as the initial morphology of the

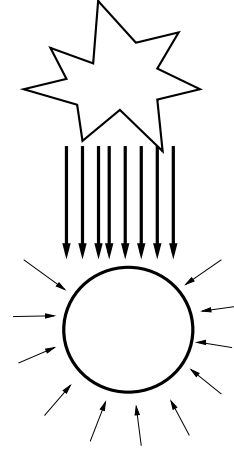


**Figure 1.** The initial geometric and the surrounding UV radiation configurations. The heavy arrow lines represent the strong Lyman continuum flux from the massive stars above the molecular cloud and the short arrow lines represent the isotropic FUV radiation ( $h\nu < 13.6 \text{ eV}$ ) flux from the interstellar medium environment.

molecular cloud. The geometrical evolution of an initially spherical molecular cloud under the effect of external environments may provide a platform for us to investigate the influence of the external radiation field on the morphology of the cloud. For investigation of the star formation at the tips of Eagle Nebula fingers, it is the dynamical evolution of the head structure that we are interested in, therefore the above assumption on the initial shape of the simulated molecular cloud should be reasonable. The mass of the cloud is uniformly distributed through a sphere of radius  $R$ . In the simulation we choose the middle finger of the Eagle Nebula as an example since it has a simpler structure than the other fingers (White et al. 1999). The initial geometric and UV radiation field configurations of the simulated cloud are shown in Figure 1.

For the head structure of the middle finger of the Eagle Nebula, with a mass  $\sim 31 \text{ M}_\odot$  and a temperature of 20 K, the Jeans length  $R_J = 0.2 \text{ pc}$ . However the radius of the head structure is about 0.1 pc, which means that the structure is unstable against the self-gravity of the cloud according to Jeans criteria. A simple SPH simulation reveals that it would collapse in  $< 10^5$  years.

However it is well known that molecular clouds are supported by turbulent and magnetic pressures in addition to the thermal pressure  $P_{\text{th}} = nkT$ . In the case of the Eagle Nebula, the observational results conclude that a large-scale ordered magnetic field is not likely to produce sufficient internal pressure balancing the external pressure and there may be a disordered component of magnetic field which provides an isotropic pressure to balance the external pressure in the head structure (White et al. 1999). The relevant turbulent pressure  $P_{\text{tb}}$  and the induced isotropic pressure  $P_B$  due to magnetic field are related to the thermal pressure by two dimensionless parameters (Gorti & Hollenbach 2002),

$$\alpha = \frac{P_{\text{tb}}}{P_{\text{th}}}; \quad \beta = \frac{P_B}{P_{\text{th}}} \quad (14)$$

The internal pressure of the molecular cloud then consists of three terms:

$$P = (1 + \alpha + \beta) P_{\text{th}} \quad (15)$$

Observations of molecular clumps in star-forming regions (Jijina et al. 1999) indicate that the values of  $\alpha$  range from about

0 in cold, dark clouds to  $\geq 2$  in regions of massive star formation. There is also observational evidence to suggest that turbulent support in clumps decreases on the smaller scales of star-forming clumps ( $r_{c,0} \leq 0.2$  pc), where  $\alpha \leq 2$  (Goodman et al 1998). Therefore we adopt the value of  $\alpha = 2$  in our simulations considering the actual diameter of the condensed head at the tip of the middle finger is 0.2 pc.

Measurements of magnetic fields and hence  $\beta$  are difficult to make, but present observational data suggest a wide range of values for  $\beta$ , ranging from 0 to a few (Crutcher 1999). We take  $\beta$  as a parameter in our simulations and determine a proper value of  $\beta$  for the Eagle Nebula so that the total internal pressure can balance the self-gravitation when the UV radiation has not been switched on in order to observe the effect of UV radiation triggered star formation in a molecular cloud. A value of  $\beta = 6$  is then obtained in this way.

We start with a warm spherical cloud of mass  $68 M_{\odot}$  and temperature of 60 K. The initial radius of the cloud is 0.4 pc and is assumed to have an uniform mass distribution and zero velocity distribution. The boundary condition adopted is of constant external pressure which corresponds to an external medium composed primarily of atomic hydrogen with  $n(\text{HI}) = 10 \text{ cm}^{-3}$  and  $T = 100$  K.

With these implementations to the original SPH code, we have developed a comprehensive three dimensional SPH code of the radiation driven implosion effects of young stars on their natal molecular clouds, which allows a detailed investigation on both dynamical and thermal evolution of a molecular cloud under the effects of nearby massive stars in a more accurate and realistic way than other existing models, because our model self-consistently includes most of the necessary physical processes which are universal in astrophysical environment.

In the following subsections, we present and discuss the results from the simulations based on the above described model with 20,000 simulated particles applied.

### 3 RESULTS AND DISCUSSION

#### 3.1 The dynamical evolution of the simulated molecular cloud

Figures 2,3 and 4 together show the number density evolution of the spherical molecular cloud with the initial conditions stated in Section 3.2.3. The overall evolutionary process can be categorised by three different stages according to the configuration of the simulated molecular core. In order to distinguish different morphologies of the core, we define a flat/elongated core as an object whose horizontal dimension is bigger/smaller than the vertical dimension.

**Flat core formation stage:** The left panel in Figure 2 shows the number density distribution of the simulated cloud at an early time  $t = 4300$  years. When the intensive Lyman continuum flux from nearby massive stars falls onto the surface of the upper hemisphere of the cloud (front surface) as shown in Figure 1, the gas within a thin layer at the surface of the upper hemisphere is ionised and forms an ionisation front at the front surface. The ionised gas is heated during the ionisation and the temperature increases. The increased pressure due to the temperature increase at this top layer drives an isothermal shock into the cloud, which compresses the neutral gas ahead of it (i.e., below the front surface). The contour lines at the front surface layer of the cloud in the left panel in Figure 2 show that a density gradient has built up there. The increased density in the neutral gas leads to a rapid mass accumulation to form a condensed core. In Figure 5, the accumulated mass in a volume

of  $0.2 \times 0.2 \times 0.35 \text{ pc}^3$  (similar dimensions to the condensed core at the head of the middle finger of Eagle Nebula) centered at the densest point in the cloud, is shown as a function of time over the whole simulation period. The mass accumulation rate in the specified volume is about  $93 M_{\odot} \text{ My}^{-1}$  in the first few thousand years. On the other hand, the ionised and heated gas at the cloud surface flows radially away from the surface of the cloud and forms an evaporating layer surrounding the surface of the cloud, shown as the 'atmosphere' outside of these contour lines in the left panel of Figure 2.

The above stated shock compression and gas evaporation can be observed from the surface of the rear hemisphere as well, but the effect is much weaker than that at the front hemisphere, because the heating effect of photoelectric emission of electrons from dust grains is much weaker than that of hydrogen ionisation by Lyman continuum radiation.

At time  $t = 0.666 \times 10^5$  years, the compressed layer (shock front) leading the ionisation front moves toward the rear hemisphere, while a flat core starts to form in the front hemisphere of the cloud due to the shock, as shown in the middle panel of Figure 2. During the next  $5 \times 10^4$  years, the core is continuously compressed and becomes flattened due to shock compression when  $t = 1.107 \times 10^5$  years as shown in the right panel of Figure 2.

With further compression of the core, as shown in the left panel of Figure 3, the small 'ear-like' structures (indicated by the white arrows) similar to those in the Lefloch & Lazareff (1994) simulations appear from the two sides of the cloud structure where the compressed layer meets the gas particles at the rear edge of the cloud at  $\theta \sim 90^\circ$ . A small 'nose' structure also grows from the rear edge of the cloud along the central line  $x = 0$ , which is due to the maximum ionisation effect along the surface normal direction. Although the appearance of the 'nose' structure from the central line, the morphology of the cloud and the core are still in a flat shape which is outlined by the contour lines in the left panel of Figure 3. In the next few  $10^4$  years, the 'ears' gradually merge with the 'nose' structure in the center and when  $t = 2.564 \times 10^5$  years, the 'ears' finally disappear and a flat core with a 'nose' structure along the center line, is shown in the middle panel in Figure 3. Now the whole cloud is in a quasi-spherical morphology. In the section 3.2.1, we will present a detailed discussion about the mechanism for the formation of the 'ear' and 'nose' structures.

**Elongated core formation stage:** In the next stage of the evolution of the simulated cloud, the whole molecular cloud structure gradually becomes elongated, as shown in the right panel of Figure 3 when  $t = 3.066 \times 10^5$  years. When the time  $t = 3.418 \times 10^5$  years, as shown in the left panel of Figure 4, a finger structure appears. A dense and elongated core having a radius of 0.1 pc in the plane perpendicular to the ionising flux direction and length of 0.35 pc along the ionising flux direction forms as shown in the left panel of Figure 4. The mass included in the above core is about  $31 M_{\odot}$ , and the average hydrogen number density is about  $10^5 \text{ cm}^{-3}$ . The configuration of the simulated molecular cloud at this stage is very similar to the head structure of the middle finger observed by White et al. (1999). We will further discuss other physical features of the cloud structure at this moment of time in the following sections.

**Triggered star formation stage:** When  $t = 3.675 \times 10^5$  years, a highly condensed spherical core starts to form at the head of the elongated structure due to the self-gravitation of the core, as shown in the middle panel of Figure 4. With further condensation of the gas into the center of the spherical core, the hydrogen density  $n$  in the center of the core increases dramatically, reaching  $10^8 \text{ cm}^{-3}$

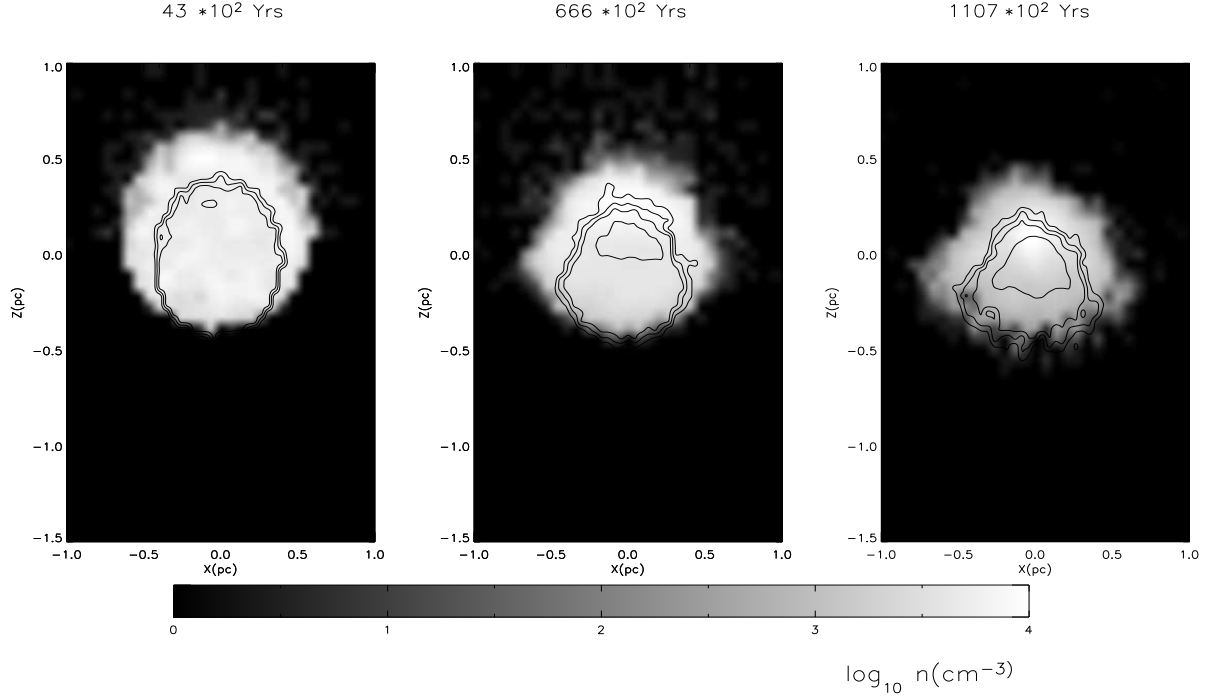


**Figure 2.** The evolution of the Hydrogen number density  $n$  ( $\text{cm}^{-3}$ ) of the simulated molecular cloud from early stages  $t = 4300$  year to  $t = 0.11$  Myr, when a flat core has formed in the front part of the cloud. The axis  $z$  is along the strong radiation flux from the massive stars, and the  $x$  axis is in the plane perpendicular to  $z$ . The initial center of the cloud is at  $(x, z) = (0, 0)$

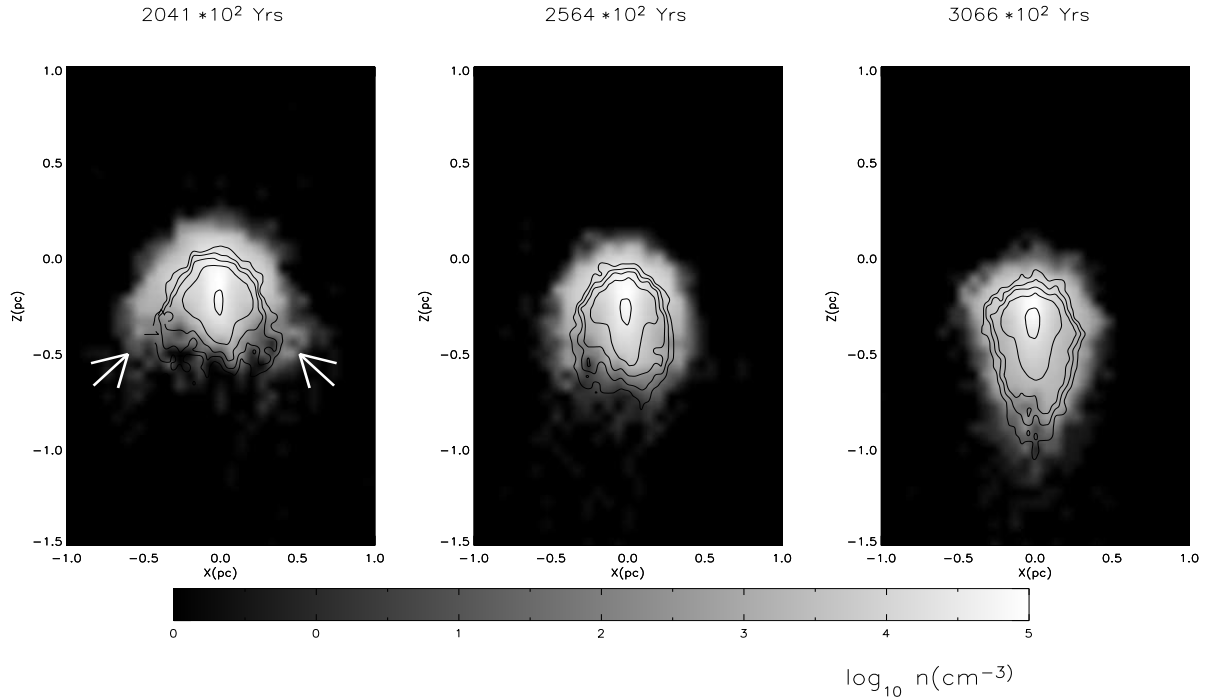


**Figure 3.** The evolution of the number density  $n$  of the simulated molecular cloud over the period of  $t = 0.2 - 0.3$  Myr, when the core gradually becomes elongated. The white arrows point to the place where the 'ear-like' structures are.

when time  $t = 3.753 \times 10^5$  years. The mass accumulated in the condensed elongated core ( $0.2 \times 0.2 \times 0.35 \text{ pc}^3$ ) reaches  $34 M_{\odot}$  when  $t = 3.753 \times 10^5$  year through compression by the isothermal shock induced by the ionising radiation, which causes the mass to condense and then collapse into the center by gravitation, i.e., triggers

the next generation of star formation in the center. The material in the condensed core quickly collapses into a smaller sphere of radius of  $0.06 \text{ pc}$  and a mass of about  $25 M_{\odot}$ .

The final mass of the whole finger structure is  $60 M_{\odot}$ . In the whole evolutionary process, the molecular cloud has lost a mass of

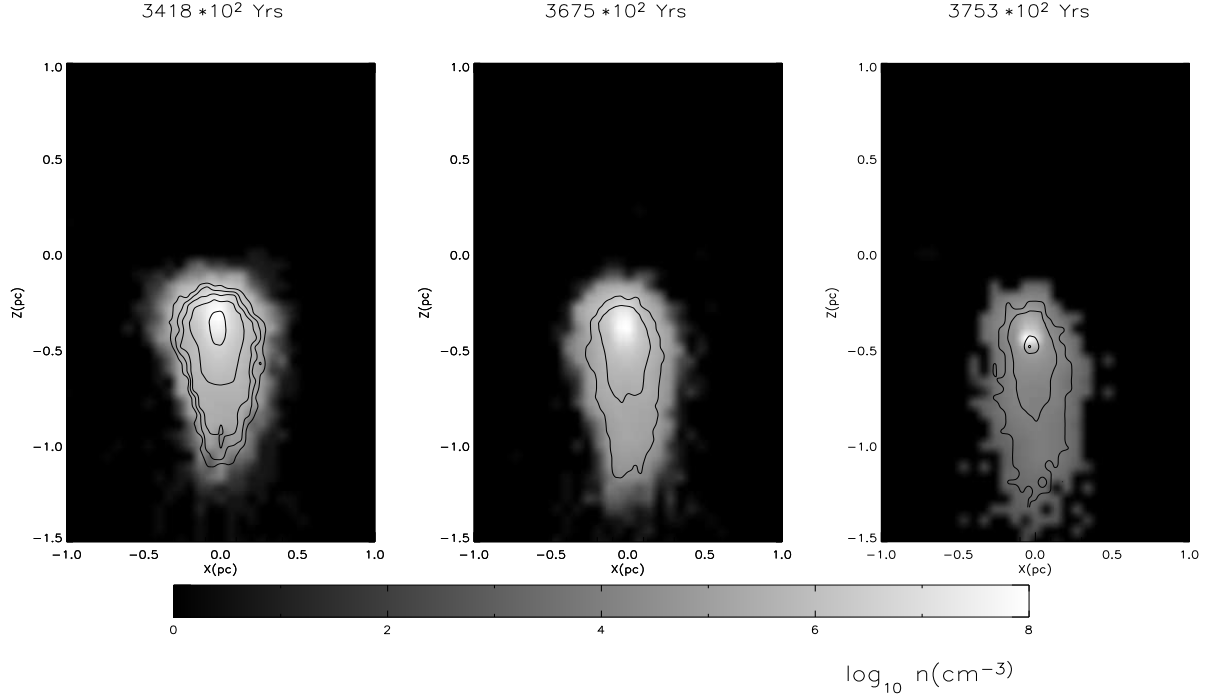


**Figure 4.** The final evolutionary stages of the condensed core collapsing into triggered star formation after 0.375 Myr.

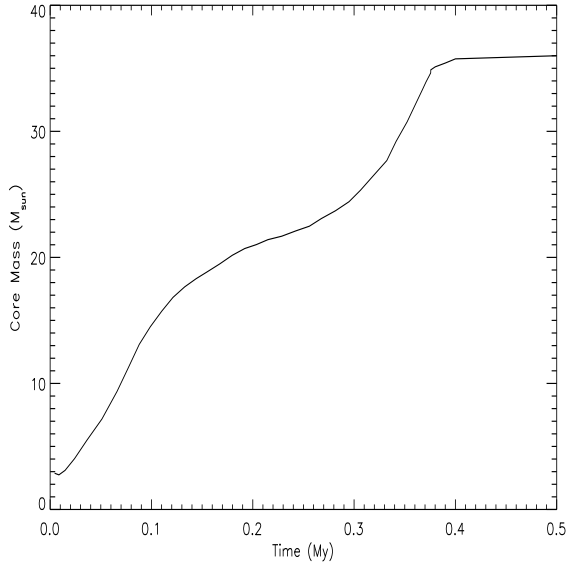


**Figure 5.** The Evolution of mass accumulated into the core of dimension  $0.2 \times 0.2 \times 0.35 \text{ pc}^3$  centered in the densest point in the simulated molecular cloud.

$8 M_{\odot}$  through photoevaporation over 0.39 My, which results in an average mass loss rate of  $\frac{8}{0.39} \sim 20.5 M_{\odot} \text{ My}^{-1}$ . This value is similar to  $21 M_{\odot} \text{ My}^{-1}$  which was obtained by Lefloch's simulation (Lefloch & Lazareff 1994). In the next section, we will discuss the mechanism for the appearances of different morphologies of the cloud during the evolution of the cloud.

### 3.2 The dynamical evolution of the cloud structure

By observing the changes in the morphology of the cloud structure, we are interested in the features of growth of the 'ears' and 'nose' structures and also the time durations for the cloud structures to stay in the 'flattened core' and 'enlongated core' stages. We will discuss them by examining the evolution of the configuration of the velocity field shown in Figure 6, which reveals an approximate evolutionary picture of the momentum of the cloud structure.

#### 3.2.1 The growth of the 'ears' and 'nose' structures

At early evolutionary stages, while the ionised gas at the top layer of the front surface of the spherical cloud is heated and evaporated from the surface, an isothermal shock travels in the opposite direction towards the rear part of the cloud and compresses the neutral gas ahead, shown as in the top left panel in Figure 6. The high pressure induced velocity distribution  $V_z(\theta)$  at the front surface layer is approximately given by (Lefloch & Lazareff, Lefloch & Lazareff (1994))

$$V_z(\theta) = V_z(0)(\cos(\theta))^{1/4} \quad (16)$$

where  $\theta$  is the angle at a surface point  $r = R$  from the  $z$  direction, and  $V_z(0)$  is the velocity at the point  $r = R, \theta = 0$ , which is  $7.5 \text{ pc My}^{-1}$  ( $7.4 \text{ km s}^{-1}$ ) at the time  $t = 4300$  years. The gas close to the symmetry axis ( $x = 0$ ) has a smaller  $\theta$  at the front surface layer will move forward faster than gas which lies further away (larger  $\theta$ ) from the axis  $x = 0$ . This velocity gradient over  $\theta$  causes the deviation of the morphology of the front surface of the cloud from the hemisphere, i.e., the front surface of the hemisphere becomes squashed, which can be seen from the middle panel in Figure 2.

The gas particles close to the outermost parts of the cloud ( $\theta \sim 90^\circ$ ), as shown in the top-middle and top-right panels in Figure 6 obtain an extra velocity along the  $z$ -direction due to the non-radial isothermal shock compression, so that they intersect the rear edge

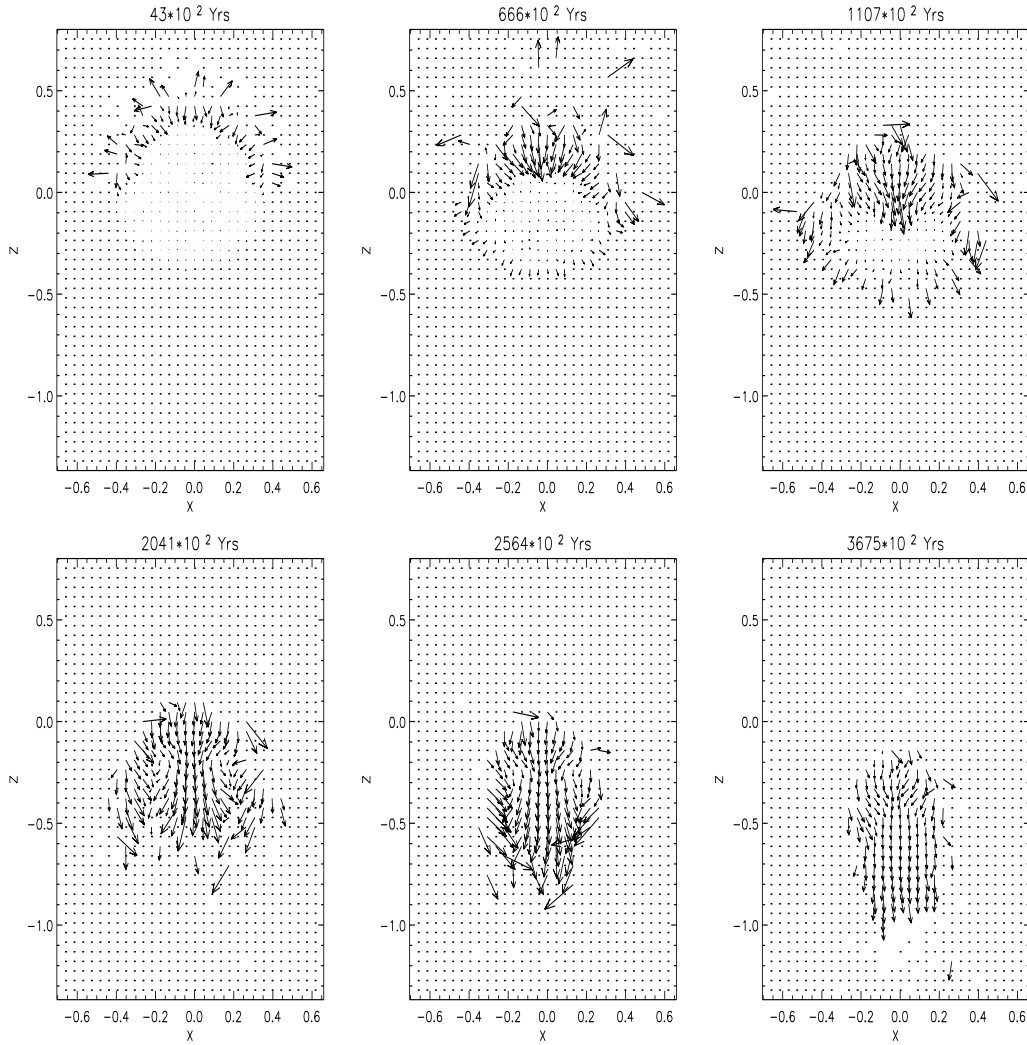


**Figure 6.** The velocity field evolution of the simulated cloud over a period time of 0.37 Myr. The length of the arrows indicates the magnitude of velocity and the longest arrow represents a velocity of  $+28 \text{ km s}^{-1}$ .

of the cloud and form the 'ear-like' structures on the two sides of the cloud, which is shown in the left panel of Figure 3

Also the gas near the symmetry axis ( $x = 0$ ) progresses forward to the rear hemisphere much faster than that further from the symmetry axis due to its higher velocity obtained from the radiation induced compression, so that a 'nose' gradually grows out from the shock front along the  $x = 0$  axis over the next  $0.44 \times 10^5$  years, dragging the most of the mass of the cloud with it, as shown clearly in the right-top panel of Figure 6.

In the following evolutionary stages, after the gas in the ears passes the front hemisphere they will merge into the moving nose structure along  $x = 0$  axis because the effect from the ionisation flux is greatly decreased inside the core region and the gravitational force of the nose structure becomes more important so that the gas in the 'ears' converges into the 'nose' structure. This effect can be seen from the bottom-left and bottom-middle panels of Figure 6 by the directions of the velocities of the gas in the 'ears' pointing to the nose. The 'ears' merging with the moving 'nose' gradually creates the tail structure of the cloud complex.

The average velocity gradient in the dense core in the left panel of the Figure 4 (which corresponds to the current state of the observed head structure of the Eagle Nebula) is  $\frac{\partial v}{\partial r} \sim 1.88 \text{ km s}^{-1} \text{ pc}^{-1}$ , which is consistent with the observed value of  $1.7 \text{ km s}^{-1} \text{ pc}^{-1}$  (White et al. 1999). The compressed gas left in the head of the cloud complex now has reached a density which exceeds its Jeans density so that it collapses into a dense core to form a new star there, while the whole cloud complex keeps moving forward along the  $-z$  direction due to the 'Rocket effect' (Oort & Spitzer 1955) arising from the evaporating gas leaving the front surface of the cloud, as shown in the bottom-right panel of Figure 6. This 'Rocket effect' makes the mass center of the cloud complex move a distance of  $0.4 \text{ pc}$  over a period of 0.37 My.

### 3.2.2 The duration of the flat and elongated morphologies

Some of the above morphological features can be found in the Lefloch & Lazareff (1994) model as well, e.g., the 'ear' structures, the elongated cloud complex (or cometary) morphology formed at the final stage of the evolution of the cloud. However we can not

ignore some profound differences in the simulated morphologies presented by these two models. Firstly in our simulations, the 'ear' structures does not last as long as in Lefloch & Lazareff's model, which we think may be the consequences of a) inclusion of gravitation in our model and b) the 3 dimensionality of our model, so the gas in the 'ears' in our model converges into the symmetry axis  $x = 0$  much earlier than that in Lefloch & Lazareff's model (which is clearly seen by the directions of the velocities of the gas at two sides), which results in the fact that the cloud complex stays longer at a flat-core morphology in our simulations. As can be seen from Figure 2–4, the ratio of the time for the cloud complex staying in flat-core morphology to that in the elongated-core morphology is  $\sim \frac{2.4}{3.9} \sim 62\%$ , which means that the simulated bright rimmed cloud spends 63% of its lifetime in a type A (with a flat core) morphology, and  $\sim \frac{3.9-2.4}{3.9} \sim 37\%$  of that in type B and C (with an elongated core), before it develops further to form cometary structure or collapse to form a new star. We reach a similar conclusion from the results of a series of simulations performed for clouds of different masses. According to the statistical average principle, the above results means that we should expect to find twice as many of flat-core BRCs as elongated-core BRCs when we observe a big group of BRCs in a similar astrophysical environment. In comparison, the relevant 2-D modelling (Lefloch & Lazareff 1994, 1995) gave a value of  $\sim \frac{0.126}{0.37} \sim 34\%$  for the time duration for the type A morphology.

The above simulated morphological sequence of the cloud complex has been validated by many observations. Sugitani et al. (1991) and Sugitani & Ogura (1994) classified their observed 89 BRCs (the SFO southern catalogue) into types of A, B and C with an increasing curvature of clouds' rim, shown as in the Figure 7, which also roughly corresponds to the three stages in our simulated BRC evolutionary morphologies. It is found that the majority of BRCs (63%) in the SFO southern catalogue are type A clouds, the remaining 37% in type B and C. Our latest radio continuum and molecular line observational study of bright-rimmed clouds reveals a very similar BRC morphological distribution to that of Sugitani et al (Urquhart et al 2003, 2005). A further investigation on the structure of BRCs, (Ogura & Sugirani 1998) supported by photoionisation induced shock models (Vanhala & Cameron 1998), also suggested that the above three morphological BRC types are possibly a time evolutionary sequence. Therefore the above interpretation of our simulated results on the morphological evolution of a BRC can be well supported by observations. The value of 63% for the ratio of the number of flat-core BRCs to that of elongated-core BRCs is consistent with the observational value 66%.

In order to further assure the role of the gravity played in the triggered star formation process within the BRC's, we repeat the simulation without including gravity in the code, the result reveals similarities to those from Lefloch & Lazareff (1994) and Williams et al. (2001) simulation, i.e., a) the core has a shorter time duration in a flat core morphology than that with gravitation included; b) the core will not collapse and after 4–5  $10^5$  years it stays in an equilibrium state with an average number density of  $10^5 \text{ cm}^{-3}$  and a central density up to  $10^6 \text{ cm}^{-3}$ . Therefore self-gravitation of the cloud indeed plays an important role in triggered star formation under the influence of UV radiation field. We will present more simulation results and analysis in our next paper for the discussion of the relationship between the morphology of the BRCs to cloud's initial structures.

### 3.3 The propagation of shock and the ionization front

An important issue in the investigation of the star formation within the Eagle Nebula fingers is to examine whether the propagation of the shock induced by the ionising radiation into the structure has triggered an irreversible collapse of the molecular cloud into a condensed center. From the simulated results, it is possible to study the propagating process of the shock by observing the evolution of the number density distribution  $n$  in the cloud structure.

In Figure 8, snapshots of the distribution of the number density  $n$  and the ionisation ratio  $x$  along the center line of the structure at different times are shown. The left panel of the first row shows that at a very early stage ( $t_1 = 0.0043$  Myr), the gas in the cloud is pushed towards the center not only from the front surface but also from the rear surface due to the surrounding weaker UV radiation from the interstellar medium. The ionisation ratio  $x$  at the front surface reaches a peak value of 0.58. Since the ionisation ratio  $x$  is linearly related to the ionising flux  $J_0$ , a sharp ionisation front is built up instantly. The hydrogen ionisation heating greatly increases the temperature at the front surface which results in a high pressure so that a strong compressive shock is formed at the front surface of the structure, as shown in the right panel of Figure 8. The bottom two panels show that the shock continues leading the ionisation front into the cloud center at  $t_3 = 0.11$  and  $t_4 = 0.2$  Myr respectively.

Overall, the head of the finger becomes denser and denser under the effect of the ionisation induced shock compression. With the increased density towards the center of the head, the ionising flux decreases very quickly ( $J(z) \sim J_0 e^{-\sigma n(1-x)z}$ ), which results in a rapid drop of ionisation ratio  $x$  inside the head structure.

If we define the region with highest density in the density profile as the shock front, the average speeds of the shock front are  $v_s = 0.33, 0.22$  and  $0.15 \text{ km s}^{-1}$  over the three periods of  $t_2 - t_1, t_3 - t_2$  and  $t_4 - t_3$ , while the corresponding speeds for the ionisation front are  $v_i = 0.18, 0.165$  and  $0.056 \text{ km s}^{-1}$  respectively. It is shown that the propagations of both shock and ionisation fronts slow down because of the increased density ahead. Since the ionisation front speed  $v_i < v_s$ , so the gap between the ionisation front and the shock front slowly increases. After  $t \sim 0.36$  Myr, the gap reaches a value of 0.125 pc, which is consistent with the fact that the peak submm continuum emission from the clumps is located at about 0.1 pc deeper into the fingers than their photoionised front surface White et al. (1999). In the following section, more details about this displacement will be discussed.

### 3.4 The evaporation of the ionised gases - HII region

While the ionising radiation induced shock precedes the ionising front into the cloud structure, the ionised hydrogen atoms at the top layer of the upper-hemisphere are heated, evaporated and move away from the front surface of the cloud to form a HII region around the front surface of the cloud. Although the gas at the other sites of the surface other than the front sites are heated as well by the surrounding environmental FUV radiation through the photoelectric emission from the surface of dust grains, the heating effect is much weaker (due to the low abundance of the dust grains) when compared with that of hydrogen ionisation so that the evaporating envelope is much thinner than that surrounding the front surface, as shown in Figure 2–4.

The panels in the upper row in Figure 9 show the movement of this evaporating layer for the first few snapshots of  $t = 0.0043, 0.009$ , and  $0.015$  Myr. The average evaporation speed is about  $25 \text{ km s}^{-1}$ . From the bottom panels of the same figure, we can see that

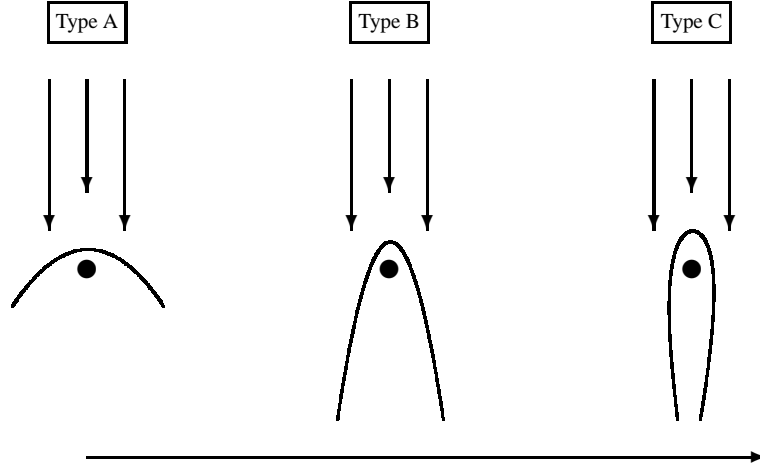


**Figure 7.** The schematic of three BRC morphologies. The vertical arrows represent the incoming ionising photon flux and horizontal arrow expresses the direction of the possible time-evolution of the cloud complex under the influence of the ionising radiation flux. The three types A, B and C correspond to the three morphologies in three different stages over the evolutionary of the cloud complex.

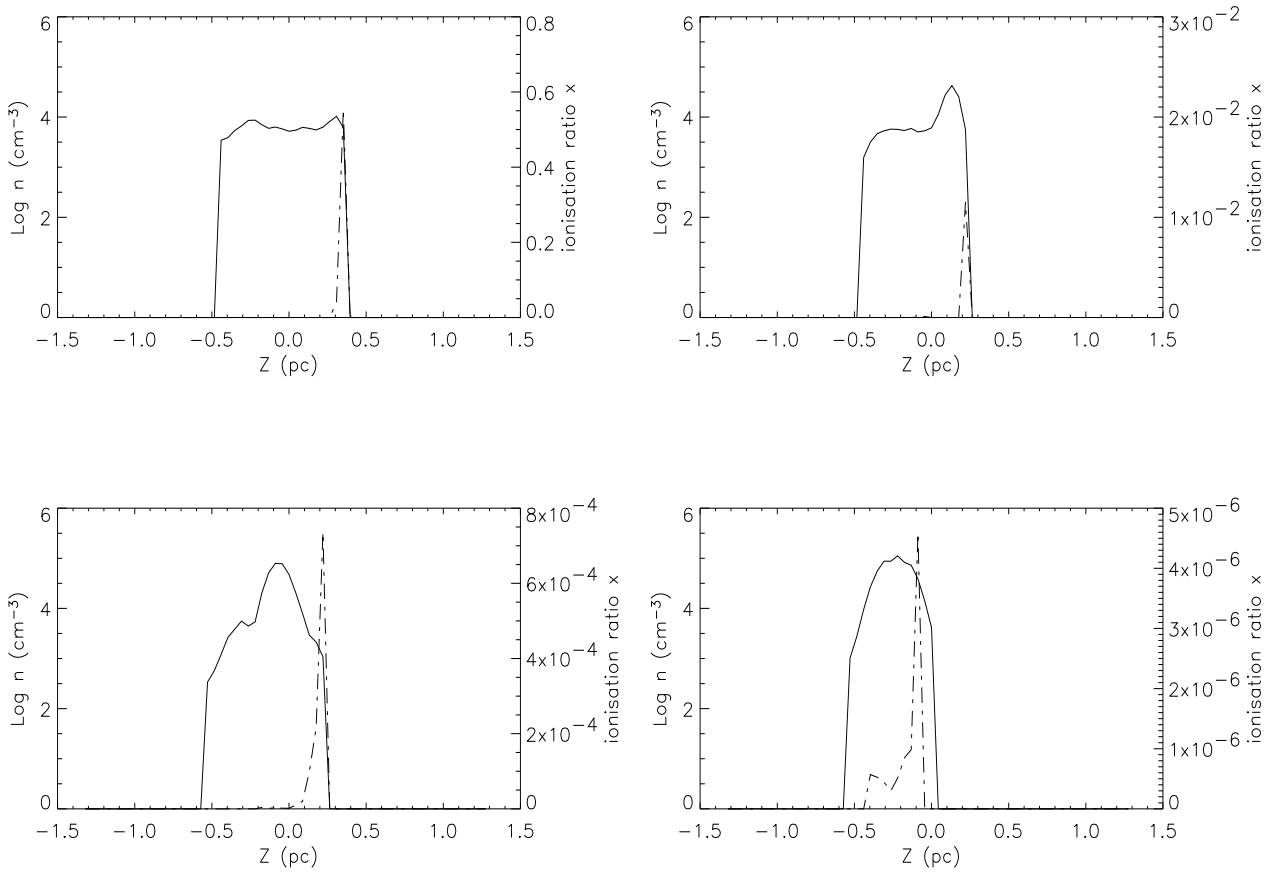


**Figure 8.** A shock (solid line) is leading the ionisation front (dot-dashed line) moving into the molecular cloud. From left to right, up to the bottom are the density distributions in the cloud along the symmetrical axis  $x = 0$  for the time  $t = 0.0043, 0.067, 0.11, 0.2$  Myr respectively.

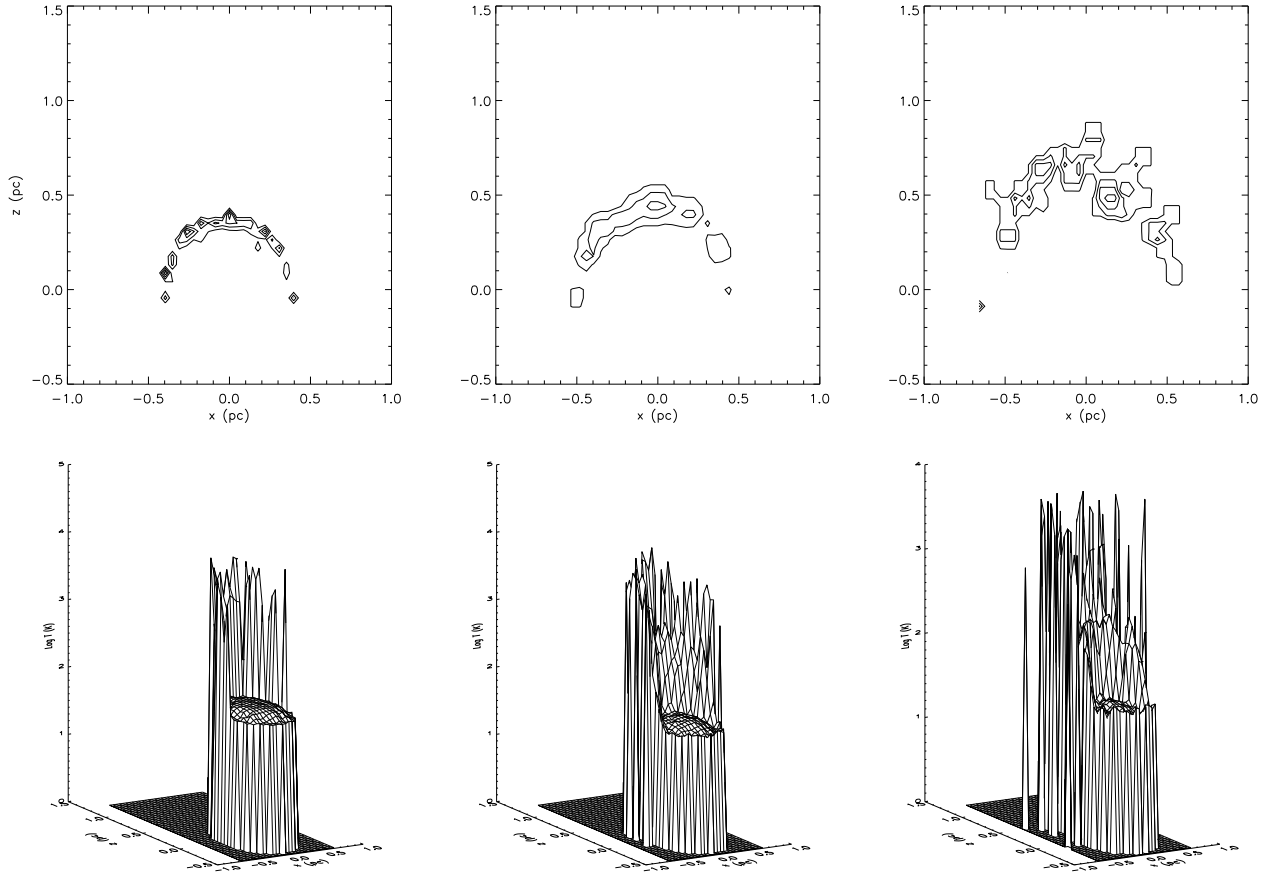


**Figure 9.** Top row: The ionised hot gas is leaving the upper semi-spherical surface. The contours are the values of the ionisation rate  $x$ , the biggest value is 0.58. The left, middle and right panels are the ionisation rate distributions in the evaporating layer over the head of middle finger of the Eagle Nebula at times 0.0043, 0.009 and 0.015 Myr respectively. Bottom row: The temperature ( $\text{Log } T$  (K)) distribution in the ionised hot gas over the same period of times.

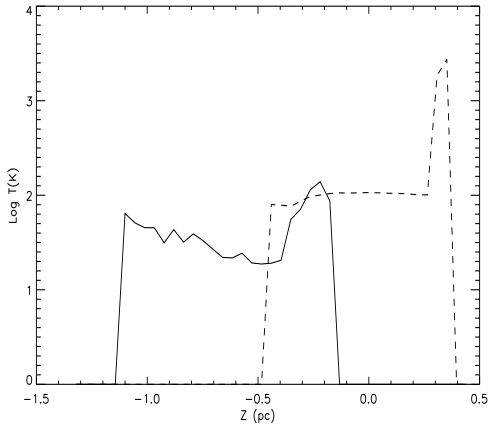


**Figure 10.** The temperature distributions at the initial and late stages of the evolution. Dashed line is for  $t = 0.0044$  Myr, and the solid line is for  $t = 0.32$  Myr

the temperature of this evaporating layer is about several  $6 \times 10^3$  K, for which Hester et al. (1996) estimated a value of  $10^4$  K, and White et al. (1999) gave a value of 6700 K. The characteristics of the modelled HII region surrounding the front surface of the Eagle Nebula fits well with the observed values.

### 3.5 Evolution of the temperature profile

The evolution of the temperature distribution of the head structure at times  $t = 0.0044$  (the dashed line) and 0.34 Myr (the solid line) along the center line  $X = 0$ , are shown in Figure 10. It is seen that shortly after the ionising radiation is switched on, i.e., when  $t = 0.0043$  Myr, the top layer at the front surface is heated as a consequence of hydrogen ionisation heating, so that the temperature increases to  $\sim 6000$  K. Inside the structure the temperature is about 60 K, close to the initial temperature of the cloud, because the effect of the radiation has not yet penetrated. After the cloud has evolved for  $t = 0.32$  Myr, the temperature in the surface layer of the cloud is about 200 K, since the ionisation flux has greatly decreased at the surface of the cloud due to the ionisation absorptions in the surrounding HII regions (which is moving away from the main structure) for the recombinations of the electrons with the hydrogen ions. The temperature at the rear surface increases to a similar value, due to the FUV radiation from the surrounding interstellar medium. The combination of the value of the surface temperature ( $\sim 200$  K) and the hydrogen density ( $n \sim 5 \times 10^4$ ) yields a thermal pressure in the surface layer of the  $\frac{P_{th}}{k} = nT \sim 10^7 \text{ cm}^{-3} \text{ K}$ . The total pressure  $\frac{P}{k} \sim 7 \times 10^7 \text{ cm}^{-3} \text{ K}$  according to Eq.(15), which is in a good agreement with the observed value by Pound (1998). The temperature in the core region of  $x \times y \times z = 0.2 \times 0.2 \times 0.35 \text{ pc}^3$ , which is centered at  $(x, y, z) = (0, 0, -0.43) \text{ pc}$ , decreases to 13–18 K, below its original value of  $T = 60$  K, due to the enhanced radi-

ation extinction, and the increased cooling efficiency in this higher density region.

In summary, the temperature distribution at the time  $t = 0.34$  Myr describes a low temperature (13–18 K) core surrounded by an outer shell of warm material of temperature of 200–250 K, which matches well with the temperature characteristics of the observed head structure at the middle fingertip in the Eagle Nebula (White et al. 1999; Pound 1998).

### 3.6 The main chemical abundance evolutions

The initial conditions for all of the chemicals abundances included are the same as those described in the previous paper, with  $X(\text{C}^+) = X(\text{CO}) = X(\text{HCO}^+) = 0$  and  $X(\text{C}) = X(\text{O}) = 10^{-4}$  when the simulation starts, where  $X_i = \frac{n_i}{n(\text{H}_2)}$  (White et al. 1999). In the left panel of Figure 11, the distributions of the fractional abundances of carbon bearing species are displayed for the time  $t = 0.32$  Myr. In the densest region between  $z = -0.5$  and  $-0.3$  pc, carbon is mainly in the form of CO, which correlates with the density of  $\text{H}_2$  because its production rate scale is  $\propto n^2(\text{H}_2)$ , which makes the peak deep inside the structure. Outside the core  $z > -0.3$  pc, CI and  $\text{C}^+$  are of comparable abundance at the front edge of the cloud structure, due to an increased ionisation of CI into  $\text{C}^+$  which results in a dramatic increasing abundance of the latter. The peak of the ionisation ratio  $x$  at  $z \sim -2.7$  pc reflects the position of the bright rim. This is to say that the ionisation peak is ahead of the CO peak by a distance of 1.25 pc, which provides a very consistent description of the relationship of the CO and  $\text{H}_\alpha$  distributions inside the cloud head with the observed displacement of 0.11 pc between CO line and  $\text{H}_\alpha$  line profiles (White et al. 1999).

The distribution of the  $\text{HCO}^+$  abundance shows a non-monotonic variation over the region because its production rate is dependent on the ionisation flux, the H bearing species and CO species. Near the front edge of the structure at  $z = -0.3$  pc, these three factors makes a peak of the  $\text{HCO}^+$  production rate. Deeper inside the structure, the high abundance of CO is dominant in the production rate of  $\text{HCO}^+$ , therefore similar pattern to that of CO, which is consistent with the observations of White et al. (1999).

White et al. also found that the ratio of CI/CO abundance increases in the low column density regions. The right panel of the figure 11 shows the corresponding ratio increases dramatically in the front region of the head structure, where the density of the cloud is very low.

## 4 COMPARISON WITH THE RESULTS FROM THE PREVIOUS MODEL

Firstly, we would like to point out that the estimated cloud thermal and chemical structures presented in the previous paper ((White et al. 1999)) was based on a static model under the assumption that the cloud was under hydrostatic equilibrium, i.e., the density distribution was fixed in time. Then the temperature and chemicals profiles were estimated according to the thermal and chemical models described in the previous SPH code, which of course were not actually describe the dynamical evolution of the cloud structure.

Secondly, a dynamical simulation based the previous SPH code in the absence of the magnetic and turbulent pressures support, indicates a quick collapse of an spherical molecular cloud of

initial mass  $68 M_\odot$  and radius of 0.4 pc (or that of  $31 M_\odot$  and radius of 0.1 pc, as we have used in our previous paper (White et al. 1999) in much less than  $10^5$  years which is not a reasonable result for the Eagle Nebula complex.

Thirdly, as we have mentioned in the previous sections, the previous SPH code didn't include the Lyman continuum in the radiation field, and the consequent hydrogen ionisation heating and cooling processes so it greatly decreased the effect of radiative implosion on the bright rimmed cloud, because the temperature near the bright rim of the cloud can only be increased to 190 K by the photoelectric effect of the FUV radiation. With the inclusion of Lyman continuum radiation, the ionising heating can heat the front layer of the cloud up to 7000 K in the first few hundred years, a reasonable temperature for HII region.

Therefore the simulation based on the previous SPH code can only simulate the effect of photoelectric heating of FUV radiation on the evolutionary of the molecular cloud, not the whole evolution picture of how a ubiquitous molecular cloud under the effect nearby massive stars can evolve into a finger-like BRC with its life ending at either triggered star formation, formation of stationary cometary structure, or being evaporated totally by the nearby massive stars' radiative field. As we have shown in this paper, these effects can only be modelled via the comprehensively extended model.

## 5 CONCLUSION

With the inclusion of the Lyman continuum in the external radiation flux and hydrogen ionisation heating effect into the energy equation in the previous code, and turbulent and magnetic pressures into the internal pressure of molecular cloud, the upgraded 3D SPH model successfully describes the dynamical evolution of an initially spherical uniform molecular cloud into cometary/triggered star formation under the influence of the strong UV radiation from nearby stars plus an isotropic surrounding interstellar medium radiation, and self-gravitation of the molecular cloud.

The application of the model to an initially spherical molecular cloud of mass  $68 M_\odot$  and a temperature of 60 K results in an Eagle Nebula finger-like structure with a very dense core of a dimension of  $0.2 \times 0.2 \times 0.35 \text{ pc}^3$  and a mass of  $31 M_\odot$  at its head after 0.34 Myr. The core has an average density of  $10^5 \text{ cm}^{-3}$  and a temperature of about 13–18 K with a velocity gradient of  $1.91 \text{ km s}^{-1}$  at time  $t = 0.34$  Myr. The dense core is surrounded by a warmer layer of temperature 200–250 K. The simulated HII region is of temperature between 3–7000 K. The characteristics of the simulated chemicals distributions are: a) CO abundance peak is 0.125 pc deeper into the core from the peak of ionisation fractional ratio  $x$  at the edge of the head structure; b)  $\text{HCO}^+$  abundance follows a similar pattern to CO in the core region; c) the abundance ratio of CI/CO increases with the decreases of the column density of the cloud. The above described characteristics of the simulated head structure coincide very well with the recent observational data (White et al. 1999). The simulation results also shows that the core will collapse into its center after another 7800 years.

It is concluded that the radiation induced compression wave has yet to pass the head structure and that the currently observed head structure at the tip of the middle finger is a part of an object which evolved from an initially larger and warmer pre-existing molecular clump. This cloud clump has been under the effect of a strong UV radiation from nearby stars for about 0.34 Myr and is currently at a transition stage towards triggered star formation.

The simulation reveals some of the similar morphological

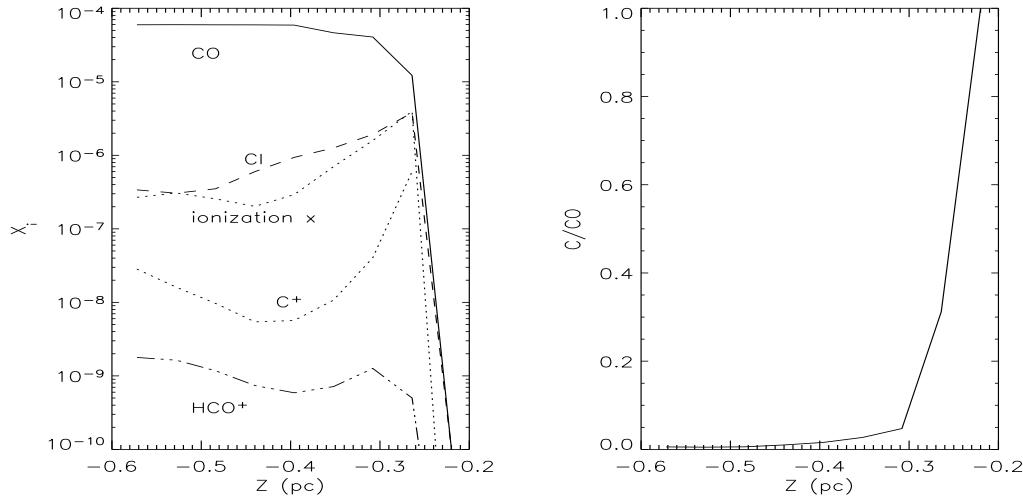


**Figure 11.** The main chemicals distributions at the time  $t = 0.34$  Myr

structures in the evolutionary process of the molecular cloud to those displayed by Lefloch & Lazareff's 2-D model and obtains a very similar estimation on the photoevaporation rate ( $20 \text{ M}_{\odot} \text{ Myr}^{-1}$  vs  $21 \text{ M}_{\odot} \text{ Myr}^{-1}$ ) from the surface of the front side, which shows the reliability of our modelling. This also shows that the Lefloch & Lazareff's 2-D model is appropriate to consider the photoevaporation of a bright-rimmed cloud, but not the issue of triggered star formation in a the cloud.

The estimation on the relative lifetimes of between type A and type B/C BRCs shows that a BRC remains in type A morphology nearly twice the time spent in the type B/C morphology, which means that we should observe double the number of BRCs in Type A morphology. This prediction agrees well with the observational results by Sugitani et al. (1991) and Urquhart et al (2003, 2005), thus provides a reasonable explanation for the observed unbalanced numbers of flat-core and elongated-core BRCs.

Comparing the above results with those based the previous SPH model, we can conclude that the hydrogen ionisation heating by Lyman continuum plays a much more important role in the dynamical evolution of a molecular cloud than that of photoelectric heating by the surrounding interstellar medium radiation. Also the inclusion of the turbulent and magnetic field pressures in the molecular cloud in the upgraded model makes the model more realistic so that it can trace the origin of an observed cloud, reveal the whole dynamical evolution process of a molecular cloud to triggered star/cometary formation under the influence of nearby stars, and predict the future evolution of the observed object.

## 6 ACKNOWLEDGEMENTS

We would like to thank the anonymous referee for his/her helpful suggestions which makes the presented work more reliable and also we learnt a lot from the communications with him/her.

## REFERENCES

- Bertoldi F., 1989, *ApJ*, 346, 735  
 Cantó J., Raga A., Steffen W., Shapiro Paul R., 1998, *ApJ* 502, 695  
 Crutcher R.M. 1999, *ApJ*, 520, 706  
 Désert F.-X., Boulanger F., Puget J.L. 1990, *A&A*, 237, 215.  
 Dyson J.E., Williams D.A., 1997, *The physics of the interstellar medium*, 2nd Edn. IOP Publishing, Bristol and Philadelphia  
 Fukuda N, Hanawa T., Sugitani Koji, 2002, *ApJ*, 568:L127-L130  
 Habing H.J., 1968, *Bulletin Astr. Inst. Netherlands* 19, 421  
 Hummer D. J. & Seaton M. J. 1963, *MNRAS*, 125, 437  
 Hurwite M., Bowyer S., Martin C. 1991, *ApJ*, 372, 167  
 Jijina J., Myers p.c., Adams F.C., 1999, *ApJ*, 125, 161  
 Goodman A.A., Barranco J.A., Wilner D.J., Heyer, M.H., 1998, *ApJ*, 504, 223  
 Gorti U., Hollenbach D., 2002, *ApJ*, 573:215-237  
 Hester J. et al., 1996, *AJ* 111, 2349.  
 Kessel-Deynet O. Burkert A., 2000, *MNRAS*, 315, 713-721.  
 Kessel-Deynet O. Burkert A., 2003, *MNRAS*, 338, 545-554.  
 Lefloch B. Lazareff B., 1994, *A&A*, 289, 559-578  
 Lefloch B., Lazareff B., 1995, *A&A*, 301, 522-536  
 Mcgaughrean M.J. and Andersen M. 2002, *A&A*, 389, 513-518  
 Nelson R.P., Langer W., 1997, *ApJ* 482, 796  
 Nelson R.P., Langer W., 1999, *ApJ* 524, 923-946  
 Ogura K., Sugitani K., 1998, *Publications of the Astronomical Society of Australia*, 15, 91  
 Oort Jan H., Spitzer L.Jr., 1955, *ApJ*, 121.  
 Osterbrock, 1974, D.E., *Astrophysics of Gaseous Nebulae*, W.H.Freeman and company.  
 García-Segura G., Franco J., 1996, *ApJ*, 469, 171.  
 Pound, Marc W. 1998, *ApJ*, 493, L113  
 Raga, A.C., et al, 2002, *A&A*, 392, 267-276,  
 Sugitani K., Fukui Y., Ogura K. 1991, *ApJS*, 77, 59.  
 Sugitani, K., Ogura, K., 1994, *ApJS*, 92, 163.  
 Sugitani K., Tamura M, Nakajima Y., et al, 2002, *ApJ*, 565: L25-L28  
 Thompson R., Smith B. and Hester J.J., 2002, *ApJ*, 570: 749-757  
 Urquhart J. S., et al., 2003, *A&A*, 409, 193-203.  
 Urquhart J.S., et al., 2005, Submitted to *A & A*.  
 Vanhala H.A.T., Cameron A.G.W., 1998, *ApJ*, 508, 291.  
 White G. J., et al. 1999, *A&A*, 342, 233-256  
 Williams, R.J.R., Ward-Thompson, D. and Whitworth, A.P. 2001, *MNRAS*, 327, 788